

Dimuon production in neutrino-nucleus collisions at next-to-next-to-leading order in perturbative QCD

Ilkka Helenius, Hannu Paukkunen and Sami Yrjänheikki

University of Jyväskylä, Department of Physics, P.O. Box 35, FI-40014 University of Jyväskylä, Finland

Helsinki Institute of Physics, P.O. Box 64, FI-00014 University of Helsinki, Finland

E-mail: ilkka.m.helenius@jyu.fi, hannu.paukkunen@jyu.fi,
sami.a.yrjanheikki@jyu.fi

ABSTRACT: Charm production in charged-current neutrino-nucleus deep-inelastic scattering (DIS), measured through dimuon final states, remains an important constraint of strangeness in global analyses of parton distribution functions (PDFs). This process has traditionally favored a smaller strange-quark PDF at small momentum fractions x than what the LHC heavy-gauge boson data have indicated. Here, we present a self-contained next-to-next-to-leading-order (NNLO) perturbative QCD calculation of dimuon production in neutrino-nucleus DIS based on semi-inclusive DIS (SIDIS). This process has been previously computed at NNLO through fully inclusive charm production. We discuss the shortcomings of this approach and how they are addressed in the SIDIS picture. We study the perturbative convergence and explore new heavy-quark production channels that become available at NNLO. We find that the NNLO corrections significantly reduce the scale uncertainties at large values of x where the cross sections are enhanced by the NNLO corrections. At small x , the NNLO corrections tend to be negative instead, which alleviate the tension between the dimuon and LHC data.

KEYWORDS: Semi-inclusive deep inelastic scattering, heavy quarks, parton distribution functions, Quantum Chromodynamics

Contents

1	Introduction	1
2	Theoretical framework	3
3	Results	5
3.1	NNLO corrections and partonic channels	5
3.2	Scale uncertainties and comparison with NuTeV data	9
4	Conclusion and outlook	11

1 Introduction

Parton distribution functions (PDFs) [1–3] and fragmentation functions (FFs) [4] are important non-perturbative inputs in applications of perturbative Quantum Chromodynamics (QCD) within the framework of collinear factorization [5]. While there has been significant advances in the first-principle calculations of PDFs [6, 7], the traditional way to determine PDFs from experimental data in global analyses is still the leading one. As of today, free-proton PDF analyses are routinely done at NNLO in perturbative QCD [8–12], with N³LO fits already on the horizon [13–16]. Nuclear PDF fits, however, are still mostly considered at NLO [17–19], although a few NNLO fits already exist [20–22]. On the one hand, this disparity has been due to a lack of precise data which would necessitate the inclusion of NNLO corrections. On the other hand, the applications of nuclear PDFs e.g. in heavy-ion collisions typically involve modeling beyond collinear factorization where the perturbative accuracy does not play such a central role. However, with the promise of new precise data, particularly from new efforts at the Large Hadron Collider (LHC), the upcoming High-Luminosity LHC (HL-LHC) [23–30], and from the Electron-Ion Collider (EIC) [31], NNLO nuclear PDFs will become increasingly relevant. For electroweak-boson production in p+Pb collisions at the LHC the NNLO corrections already exceed experimental uncertainties at certain kinematics [22].

The aim of this paper is to discuss the calculation of dimuon production in neutrino-nucleus collisions at NNLO precision. In this charged-current process, one muon originates from the beam neutrino and the other one from a heavy-flavor decay providing access to the strange-quark content of the target nucleon. While the available measurements for this process from the CCFR, NuTeV, and NOMAD collaborations [32–36], taken with heavy nuclear targets (mainly iron), date back 10 to 30 years, they still constitute an important constraint of strangeness in nuclei and for the possible strange-antistrange asymmetry. More recent constraints include e.g. inclusive and charm-tagged W and Z production

in proton-proton collisions [37–39], as well as semi-inclusive kaon production in charged-lepton-proton collisions [40–42]. There are, however, also challenges when it comes to constraining the strangeness by these processes in global analyses. In W and Z production, the high interaction scale makes it more difficult to disentangle the non-perturbative strange distribution from the perturbatively-generated strange sea. In kaon production, the precision of the kaon FFs proves to be a limiting factor. In addition, the LHC W and Z production data appear to be in tension with the dimuon data: the strange-sea suppression $(s + \bar{s})/(\bar{u} + \bar{d})$ determined from neutrino data is around 0.5 [32, 36] at $x \sim 0.02$ at factorization scale $Q \sim 1.6$ GeV, whereas the LHC data prefer an unsuppressed strange sea [43–46]. There are, however, indications [47] that the NNLO corrections will reduce these tensions, which makes it important to scrutinize these corrections.

The dimuon production $\nu N \rightarrow \mu\mu X$ is typically calculated by relating it to the inclusive charm production $\nu N \rightarrow c\mu X$ by a factorization-like formula,

$$d\sigma(\nu N \rightarrow \mu\mu X) = \mathcal{A}\mathcal{B}_\mu d\sigma(\nu N \rightarrow c\mu X), \quad (1.1)$$

where the acceptance correction $\mathcal{A} \sim 0.4 \dots 0.9$ ensures that the decay muon meets the experimentally-imposed energy cut, and $\mathcal{B}_\mu \sim 0.09 \pm 10\%$ is the average semileptonic branching ratio. This is accurate to leading order (LO) in the fixed-flavor number scheme (FFNS) — a framework in which the charm-quark is not considered as an active parton in the Dokshitzer-Gribov-Lipatov-Altarelli-Parisi (DGLAP) evolution [48–51]. Beyond LO FFNS eq. (1.1) becomes increasingly approximative and just by increasing the perturbative accuracy of $d\sigma(\nu N \rightarrow c\mu X)$ does not necessarily mean that the overall accuracy would be increased unless the acceptance correction — taken by default from a fixed-order NLO calculation [52] — is also updated to NNLO precision. Furthermore, to consistently account for the heavy-quark mass effects in association with PDFs, an appropriate general-mass variable-flavour-number scheme (GM-VFNS) should be applied in the acceptance calculation [53–64]. Nevertheless, such a factorized approximation has been applied in the NNLO calculations of the dimuon process [65, 66] and included in PDF fits [10, 11]. A conceptual issue, which first appears at NNLO, is the infrared-unsafety of inclusive charm-quark production [67]. This arises from diagrams such as the one in figure 1a which gives rise to a logarithmic contribution $\log(Q^2/m_c^2)$. In fully inclusive DIS, with no requirement of a charm quark in the final state, these logarithms would be cancelled by virtual corrections such as the one arising from the diagram in figure 1b.

Our generic approach, laid out in refs. [68, 69], resolves the aforementioned difficulties at once. The idea is to consider the entire chain of processes that lead to the dimuon production — the semi-inclusive charm-hadron production followed by its decay. On the one hand, the mass logarithms from diagrams like the one in figure 1a are resummed to the scale dependence of FFs resolving the infrared unsafety discussed above. On the other hand, the non-perturbative decay of charm-hadron into dimuons is treated on rather general grounds by parametrizing the differential decay width and fitting it to the experimental data from e^+e^- collisions [70]. The differential nature of the decay width allows us to naturally evaluate the fiducial cross sections in the decay-muon kinematics, making the separate acceptance correction required in eq. (1.1) an unnecessary concept in our framework.

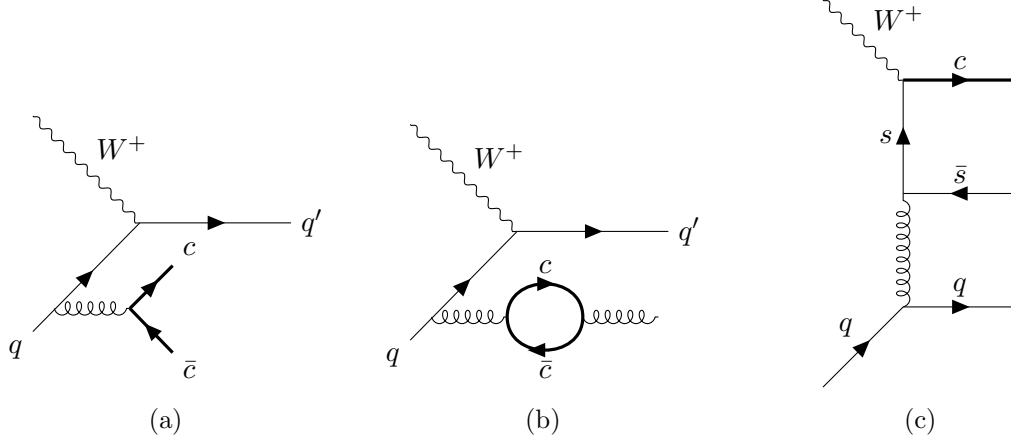


Figure 1: Examples of NNLO diagrams in neutrino-nucleus DIS.

Higher-order corrections to hard-scattering processes can sometimes entail large corrections due to the opening of new partonic channels which can compensate the suppression induced by the additional powers of the strong coupling α_s . Up to NLO, the only allowed initial-state quarks in neutrino scattering are the lower-type quarks (down, strange, bottom). Due to diagrams like the one shown in Figure 1c, the up-type quarks (up, charm) are also possible at NNLO. As the up-quark distribution is enhanced in the valence region, i.e. at large x , there could potentially be a significant contribution from the up-quark-initiated channels when approaching this regime.

2 Theoretical framework

Consider a neutrino ν with energy E_ν incident on a nucleon N at rest. The inclusive cross section for the dimuon final state $\nu N \rightarrow \mu\mu X$ with an energy cut E_μ^{\min} imposed on the muon originating from the decays of charm-hadrons h can be written in the narrow-width approximation as [68],

$$\frac{d\sigma(\nu N \rightarrow \mu\mu X)}{dx dy} = \sum_h \int dz \frac{d\sigma(\nu N \rightarrow \mu h X)}{dx dy dz} B_{h \rightarrow \mu}(E_h = zyE_\nu, E_\mu^{\min}). \quad (2.1)$$

Here, $\nu N \rightarrow \mu h X$ refers to the underlying SIDIS process $\nu_\mu(k) + N(P_N) \rightarrow \mu(k') + h(P_h) + X$, whose cross section is of the standard form,

$$\begin{aligned} \frac{d\sigma(\nu_\mu N \rightarrow \mu h X)}{dx dy dz} &= \frac{G_F^2 M_W^4}{(Q^2 + M_W^2)^2} \frac{Q^2}{2\pi xy} \\ &\times \left[xy^2 F_1(x, z, Q^2) + \left(1 - y - \frac{x^2 y^2 M^2}{Q^2} \right) F_2(x, z, Q^2) \right. \\ &\quad \left. \pm xy \left(1 - \frac{y}{2} \right) F_3(x, z, Q^2) \right], \end{aligned} \quad (2.2)$$

where M is the nucleon mass, $G_F \approx 1.166379 \times 10^{-5} \text{ GeV}^{-2}$ the Fermi constant, and $M_W \approx 80.377 \text{ GeV}$ the W -boson mass. The kinematic variables are the usual ones,

$$\begin{aligned} Q^2 &= -q^2 = -(k - k')^2, \\ x &= \frac{Q^2}{2P_N \cdot q}, \\ y &= \frac{P_N \cdot q}{P_N \cdot k}, \\ z &= \frac{P_N \cdot P_h}{P_N \cdot q}. \end{aligned} \tag{2.3}$$

The plus sign in the F_3 structure function corresponds to neutrino scattering and the minus sign to antineutrino scattering. The function $B_{h \rightarrow \mu}$ appearing in eq. (2.1) is an energy-dependent branching fraction,

$$B_{h \rightarrow \mu}(E_h, E_\mu^{\min}) = \frac{1}{\Gamma_h^{\text{tot}}} \int d^3 \mathbf{p}_\mu \frac{d^3 \Gamma_{h \rightarrow \mu}}{d^3 \mathbf{p}_\mu} \Big|_{E_\mu > E_\mu^{\min}}, \tag{2.4}$$

where Γ_h^{tot} is the total decay width of the hadron h and the integration is over the decay-muon momentum \mathbf{p}_μ with the muon energy E_μ restricted above the cut E_μ^{\min} as typically required in experimental analyses. The generic form of the differential decay width, dictated by Lorentz invariance, can be written as,

$$\frac{d^3 \Gamma_{h \rightarrow \mu}}{d^3 \mathbf{p}_\mu} = \frac{d_{h \rightarrow \mu}(w)}{2m_h E_\mu}, \quad w = \frac{p_\mu \cdot P_h}{m_h^2},$$

where m_h is the mass of h . The Lorentz-invariant decay function $d_{h \rightarrow \mu}(w)$ has been parametrized and fitted [68] to data from e^+e^- collisions [70]. The structure functions appearing in eq. (2.2) are generic convolutions between PDFs f_i , hard coefficient functions C_{ij} , and FFs D_i ,

$$F_i(x, z, Q^2) = \sum_{ij} \int_{\chi_n}^1 \frac{d\xi}{\xi} \int_z^1 \frac{d\zeta}{\zeta} f_i \left(\frac{\chi_n}{\xi}, \mu_{\text{fact}}^2 \right) C_{ij}(\xi, \zeta, Q^2, \mu_{\text{ren}}^2, \mu_{\text{fact}}^2, \mu_{\text{frag}}^2) D_j \left(\frac{z}{\zeta}, \mu_{\text{frag}}^2 \right), \tag{2.5}$$

where μ_{ren}^2 is the renormalization scale, μ_{fact}^2 the factorization scale, and μ_{frag}^2 the fragmentation scale. By default, we take $\mu_{\text{ren}}^2 = \mu_{\text{fact}}^2 = \mu_{\text{frag}}^2 = \mu_0^2 = Q^2 + m_c^2$. The slow-rescaling variable χ_n ,

$$\chi_n \equiv x \left[1 + \frac{(nm_c)^2}{Q^2} \right], \tag{2.6}$$

where n is the number of final-state charm quarks, accounts for the additional kinematical restriction set by the charm-quark masses — see ref. [69] for more details. The coefficient functions C_{ij} are not unique but they depend on the chosen GM-VFNS variant. Up to NLO, $\mathcal{O}(\alpha_s)$, our calculation here takes them in the so-called SACOT- χ scheme [53–60, 62–64], explained thoroughly in ref. [69], which reduces to the usual zero-mass $\overline{\text{MS}}$ scheme in the limit $Q^2 \rightarrow \infty$. The new ingredients here are the NNLO corrections for which we

use the massless coefficient functions provided in ref. [71]. This effectively means that we implement them in what can be called the slow-rescaling (SR), or intermediate-mass (IM), approximation [72]. As we learned in ref. [69], the kinematic mass corrections that are effectively induced by the slow-rescaling variable, are clearly the dominant ones up to NLO, apart from very low values of $Q^2 \sim m_c^2$ which are always excluded from global PDF fits. Thus, it is reasonable to expect that in the relevant region of Q^2 our framework should capture the dominant NNLO corrections.

Along with the size of the perturbative corrections, the dependence of the cross sections on the renormalization, factorization, and fragmentation scales is typically taken as a measure of perturbative convergence. To faithfully study this aspect in our setup, we should also use PDFs and FFs that respect the DGLAP evolution with NNLO splitting functions. For the PDF, we use the TUJU21 set [22] of nuclear PDFs (iron, $A = 56$) which also dictates our choice for the charm-quark mass $m_c = 1.43$ GeV. Unfortunately, no applicable NNLO FFs currently exist.¹ In our preceding studies [68, 69] we have used the GM-VFNS NLO sets `kkks08` (specifically, the OPAL set) [74] for D^0 and D^+ and `bkk05` [75] for D_s and Λ_c^+ . In lieu of a proper NNLO fit, we take the analytic NLO parametrizations of these analyses and simply redo the evolution at NNLO using the EKO framework [76, 77]. It is important to note that simply redoing the evolution does not constitute a proper NNLO analysis, but should be sufficient for studying the scale dependence. An additional complication at NNLO is the need for matching conditions in PDF and FF DGLAP evolution when crossing either the charm- or bottom-mass threshold, where the number of active quark flavors N_f changes. Unlike at lower orders, the NNLO coefficient functions depend explicitly on N_f , making them discontinuous at the thresholds. This discontinuity should then be compensated in the evolution of the strong coupling α_s , PDF, and FF, which also turns these objects discontinuous. In the end, all these discontinuities should cancel so that the cross sections are continuous, though the cancellation is of perturbative nature and therefore numerically incomplete. However, the time-like matching conditions are not fully known at NNLO [78]. Therefore, they are not implemented in EKO and are not included in our NNLO FFs. As a consequence, the discontinuity at the bottom threshold can still get smaller once the FF matching conditions have been implemented.

3 Results

3.1 NNLO corrections and partonic channels

To understand the impact of NNLO coefficient functions, the upper panels of figures 2 and 3 display the neutrino and antineutrino cross sections calculated without (left) and with (right) the NNLO corrections. The kinematics correspond to those of the NuTeV experiment. In both cases, the effect of the NNLO terms is to somewhat decrease the cross sections at small values of x , while at large x the cross sections grow. Qualitatively similar behaviour has been observed in inclusive charm production [66]. The overall effect

¹The initial scale of the D^0 and D^+ fit in ref. [73] is above the bottom-mass threshold, which is too large for our purposes.

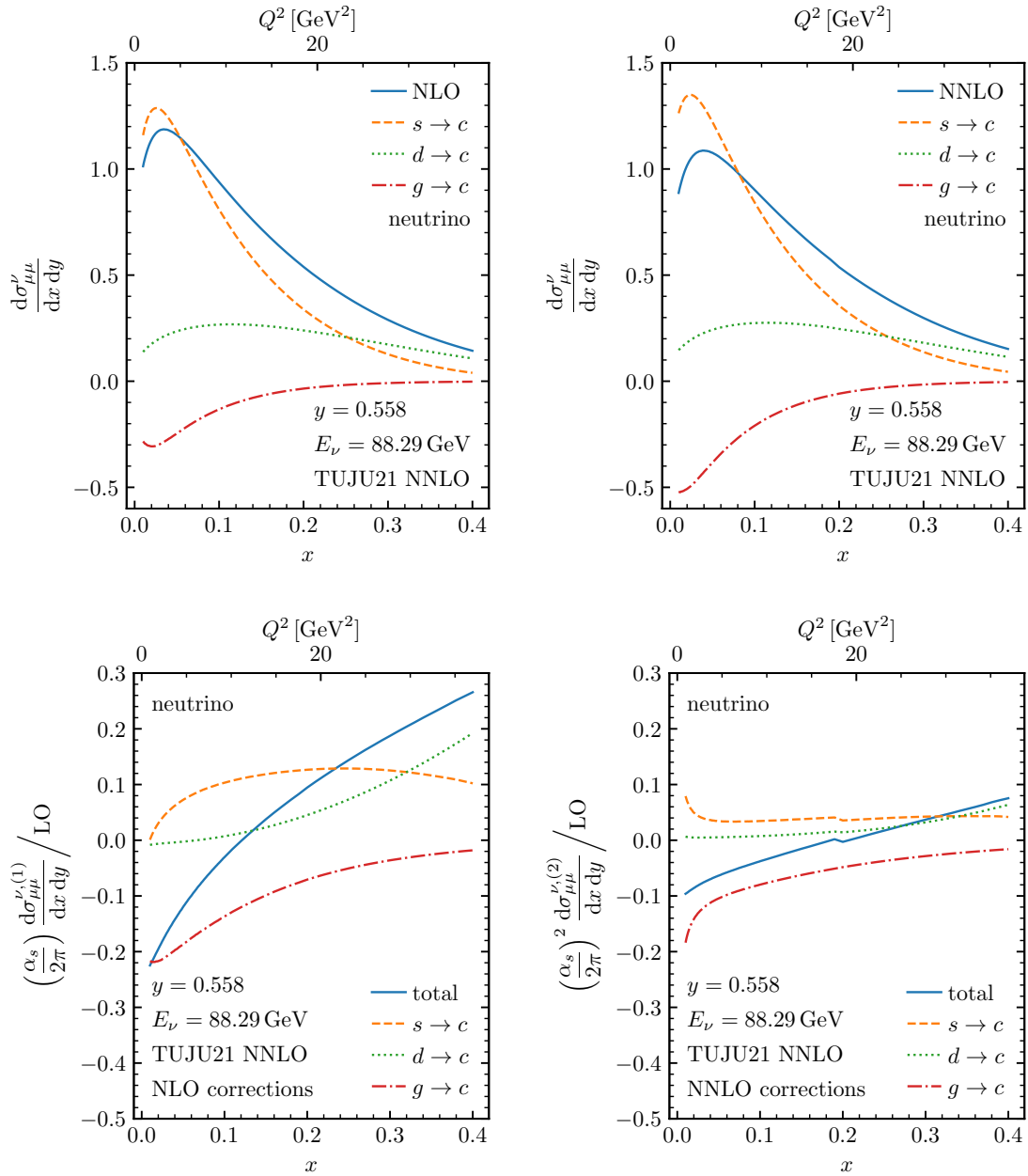


Figure 2: Dimuon cross sections in neutrino-nucleus DIS at NLO (left) and NNLO (right) together with the leading-channel contributions. The upper panels show the full cross sections, while the lower panels show the corresponding perturbative corrections normalized to the full LO cross sections. All contributions are computed with NNLO PDF and FFs, as described in section 2.

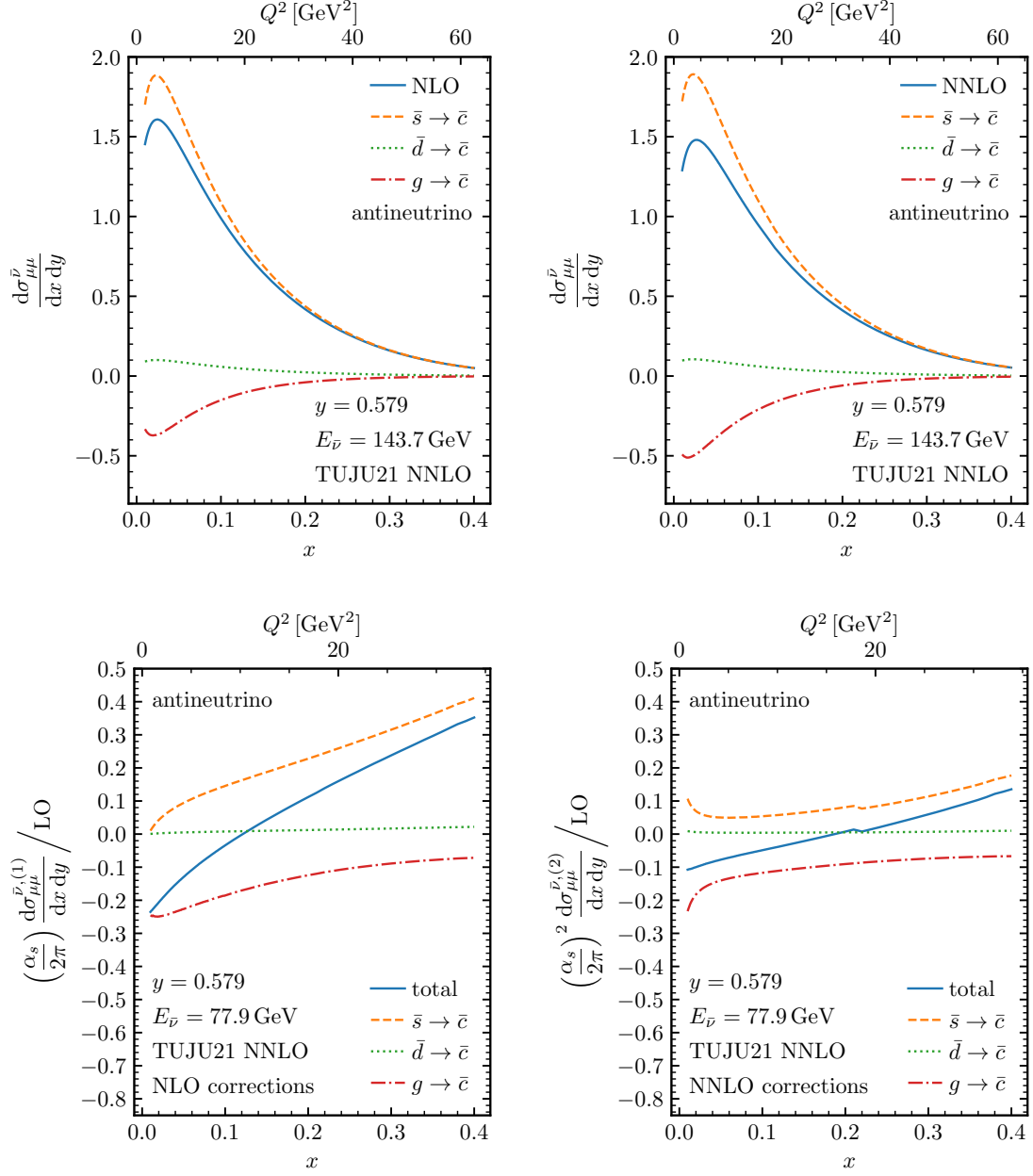


Figure 3: Same as figure 2, but for antineutrino scattering.

is, however, rather mild. While the exact numbers of course depend on the PDFs and the kinematics, the trend itself holds generally in the entire kinematic region covered by the existing NuTeV and CCFR measurements. The upper panels of figures 2 and 3 also show the contributions of the most relevant partonic channels. For neutrino scattering these are $s \rightarrow c$, $d \rightarrow c$, and $g \rightarrow c$, i.e. the ones that are initiated by a down quark, strange quark, or a gluon, and in which the fragmenting parton is the charm quark. Of the quark-initiated channels, the strange-initiated channel is typically more important due to the hierarchy in the Cabibbo-Kobayashi-Maskawa (CKM) matrix elements. This, of course, is the reason why dimuon production is a good constraint for the strange-quark PDFs. Only at very large x does the down-initiated contribution become larger than the strange-initiated one due to the existence of the down-valence PDF in comparison to the strange-quark PDF with only sea-like content. No analogous valence distribution exists for \bar{d} , and therefore antineutrino scattering is entirely dominated by the $\bar{s} \rightarrow \bar{c}$ and $g \rightarrow \bar{c}$ channels. The lower panels of figures 2 and 3 compare the NLO, i.e. $\mathcal{O}(\alpha_s)$ (left), and NNLO, i.e. $\mathcal{O}(\alpha_s^2)$ (right), contributions normalized to the full LO cross section. The overall NNLO corrections are seen to be systematically smaller than the NLO ones which indicates a convergence of the perturbative series. In the NNLO corrections the expected discontinuity at the bottom-quark threshold discussed in section 2 is visible, but in the full cross sections (the upper panels) this small discontinuity can hardly be seen. We find that the NNLO corrections to the gluon-induced channels are always negative while the quark-induced ones are usually positive, and the two tend to compensate each other in the sum. However, it should be noted that only the overall correction is physically relevant as the split to the gluon- and quark-initiated contributions depends heavily on the adopted factorization scheme, and the negativity of the gluon contributions is very typical for the $\overline{\text{MS}}$ scheme [79]. Channels involving the fragmentation of a parton other than the charm quark do not have any meaningful contribution as their charmed-meson fragmentation functions are negligible due to the additional splittings needed to produce a charmed final state. The b -quark FF is larger, but the associated CKM-matrix elements quench these contributions.

As discussed in section 1, new and potentially relevant channels open up at NNLO. These contributions are shown in figure 4, which demonstrates that these new channels are, at the end, not very significant. For neutrino scattering, the most significant is $u \rightarrow c$, which is to be expected because of the large valence contribution from the up-quark distribution. Nevertheless, the contribution from $u \rightarrow c$ is still two orders of magnitude smaller than from the pre-existing channels. It should be noted that the contribution from $u \rightarrow c$ becomes negative at small x , which appears as a kink in the logarithmic plot. For antineutrino scattering, the channels $d \rightarrow \bar{c}$ and $u \rightarrow \bar{c}$ are relatively more important than in the neutrino case as the NNLO is the first order at which the valence-quark PDFs begin to contribute. The contribution from $d \rightarrow \bar{c}$ is comparable to that of $\bar{d} \rightarrow \bar{c}$ in figure 3, with the contribution from $u \rightarrow \bar{c}$ being even larger. While the corrections from these channels are still clearly subleading in comparison to $\bar{s} \rightarrow \bar{c}$ and $g \rightarrow \bar{c}$, the difference is now one order of magnitude instead of two. It should be noted that in figure 4, the contributions from the $\bar{u} \rightarrow \bar{c}$ and $s \rightarrow \bar{c}$ channels are identical. This is because these channels use the same coefficient function, and because of the constraint $\bar{s} = s = \bar{d} = \bar{u}$ used in the TUJU21

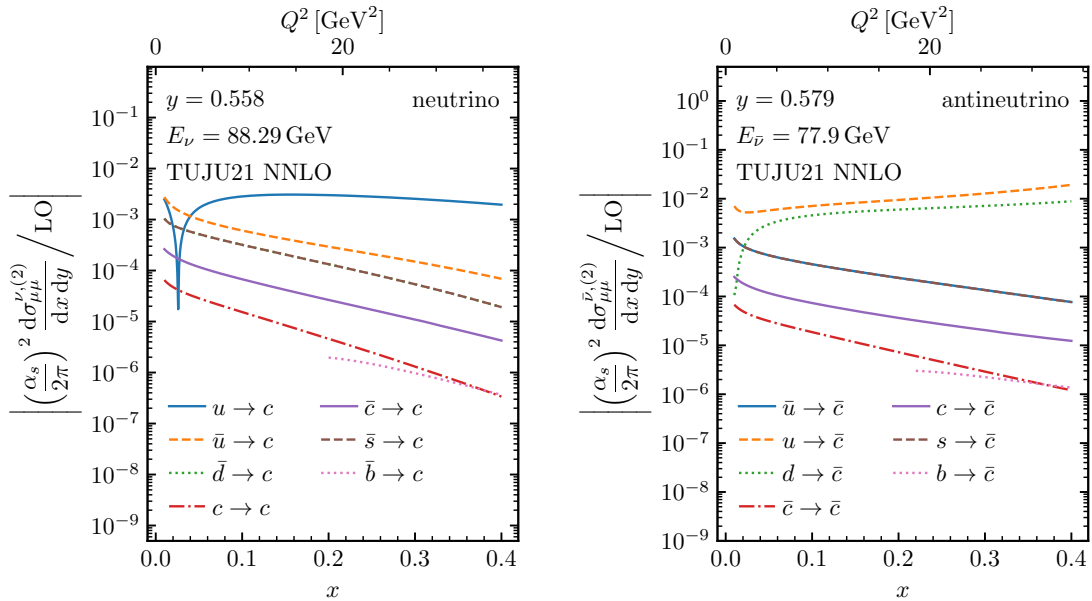


Figure 4: Subleading NNLO corrections to the dimuon cross section in neutrino (left) and antineutrino (right) scattering, normalized to the full LO cross section. The corrections are computed with NNLO PDF and FFs, as described in section 2.

parametrization.

3.2 Scale uncertainties and comparison with NuTeV data

Figure 5 shows the 17-point scale variations of the neutrino and antineutrino dimuon cross section at LO, NLO, and NNLO in the same kinematical setup as in the previous plots. We also show the corresponding experimental data from NuTeV [34]. The LO and NLO results are computed with the TUJU21 NLO PDF and the original `kkks08` and `bkk05` FFs, while the NNLO contribution is computed with the TUJU21 NNLO PDF and the NNLO FFs described in section 2. The 17-point scale variations consist of variations of the form $\mu_i^2 = \max\{k^2 \mu_0^2, m_c^2\}$, $k \in \{\frac{1}{2}, 1, 2\}$, for the renormalization scale μ_{ren}^2 , factorization scale μ_{fact}^2 , and fragmentation scale μ_{frag}^2 , with the condition $\frac{1}{2}\mu_{\text{ren}} \leq \mu_{\text{fact}}, \mu_{\text{frag}} \leq 2\mu_{\text{ren}}$. The LO scale variations are always clearly larger than the NLO or NNLO ones. At small values of x the NNLO scale variations are similar to the NLO ones but as x grows, the NNLO scale variations start to diminish, indicating a better perturbative convergence at larger x . This is to be expected as larger x corresponds to larger Q^2 and therefore to a smaller expansion parameter α_s . One could speculate that the similarity of the NLO and NNLO scale variations at small x could be related to the SR/IM approximation we make in including the NNLO terms. However, at the NLO level we did not observe a significant difference in the scale uncertainties between the SR/IM approximation and the full GM-VFNS calculation [69]. The NNLO results always land within the NLO scale-variation bands, so in this case the NLO scale variations gave a reasonable estimate on

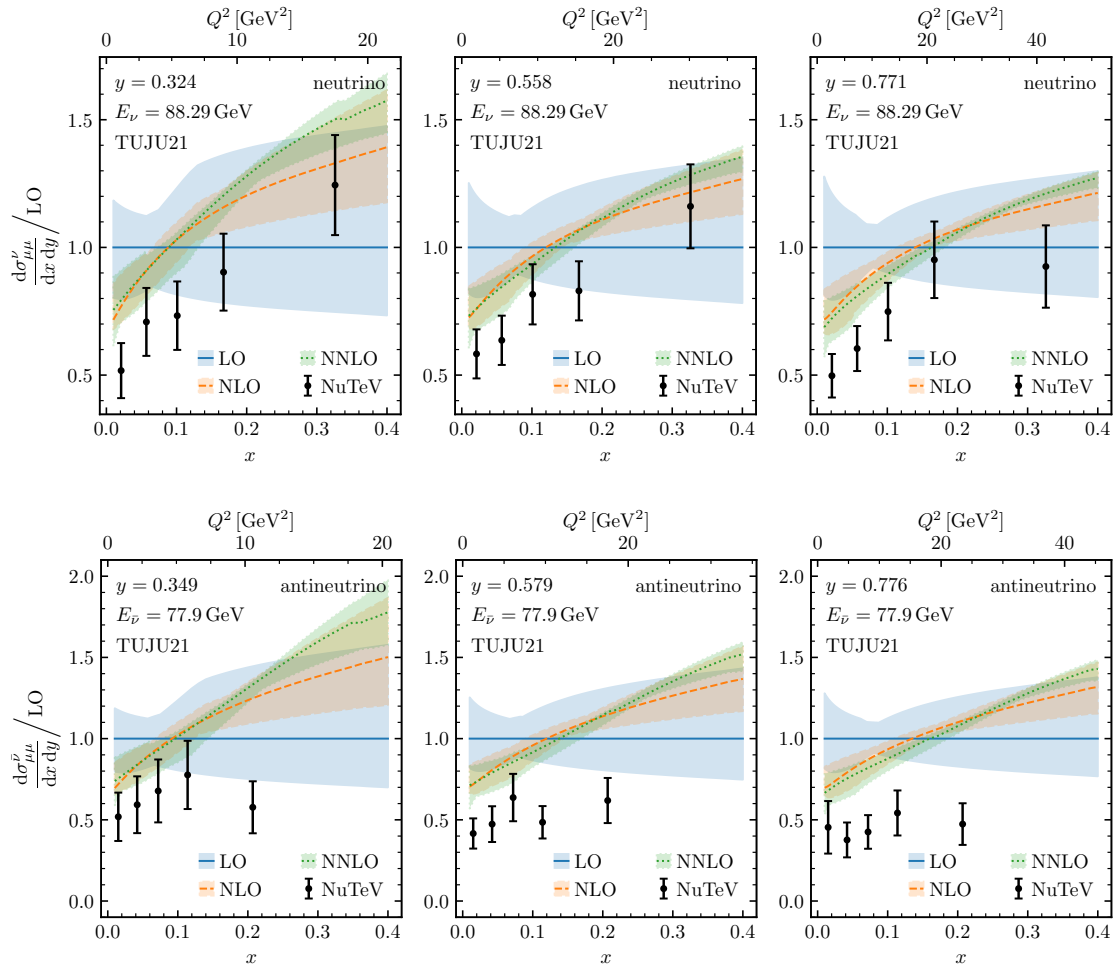


Figure 5: 17-point scale variations of the dimuon cross section in neutrino (top) and antineutrino (bottom) scattering, normalized to the LO cross section. The LO and NLO contributions are computed with NLO PDF and FFs, while the NNLO contributions are computed with NNLO PDF and FFs, as described in section 2.

the size of the missing higher-order corrections. In comparison to the NuTeV data, at small x where the NNLO calculation does not significantly reduce the scale variations, the experimental errors remain comparable to the scale uncertainties. At larger x , however, the experimental errors are notably bigger than the NNLO scale uncertainties. Figure 5 indicates that using TUJU21 PDFs for the target nucleon yields on average a 20–30 % larger cross section compared to the NuTeV data. The mismatch is more pronounced in case of antineutrino data where valence- d -originating contributions are negligible. This can be traced to the unsuppressed strangeness in the TUJU21 analysis, which assumes $\bar{s} = s = \bar{d} = \bar{u}$ at the parametrization scale. This also concretely demonstrates what we wrote earlier in section 1 about dimuon data preferring a suppressed strangeness and once more highlights the constraints these dimuon data can provide. To this end, figure 6

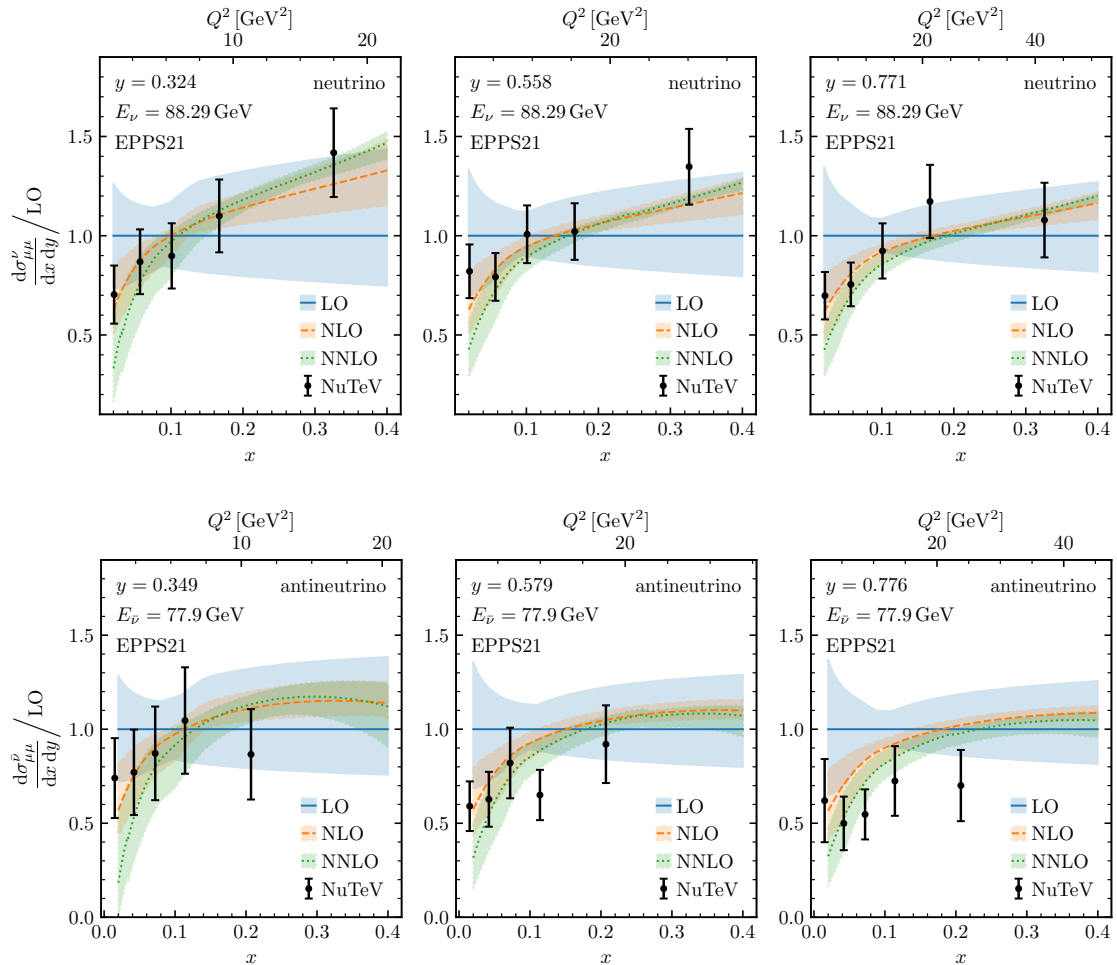


Figure 6: 17-point scale variations of the dimuon cross section in neutrino (top) and antineutrino (bottom) scattering, normalized to the LO cross section. All contributions are computed with the NLO EPPS21 PDF set and NLO FFs. The theoretical results are compared with NuTeV data.

presents the same comparison as figure 5, but this time by using the NLO EPPS21 nuclear PDF set [18]. This set of PDFs is based on the CT18ANLO set of proton PDFs [9], in which the strangeness suppression is a compromise between what these dimuon data — within a FFNS NLO calculation calculation using the factorized approximation eq. (1.1) — and the LHC W and Z data prefer. There is now clearly a better correspondence to the shown NuTeV data.

4 Conclusion and outlook

In this paper, we presented an NNLO-improved version of our NLO-level GM-VFNS implementation [68, 69] of dimuon production in neutrino-nucleus DIS, based on the zero-mass NNLO SIDIS coefficient functions calculated in ref. [71]. Despite using the zero-mass coef-

ficient functions, we properly took into account the mass dependence that is of kinematic origin and which is arguably the leading mass effect at $Q^2 \gtrsim 4 \text{ GeV}^2$. We studied the impact the NNLO corrections have on the cross sections at kinematics corresponding to available experimental data and charted the expected size of still higher-order corrections by standard scale variations. In general, the NNLO corrections were found to decrease the cross sections at small x while an enhancement was observed at large x . This behaviour appears to decrease the known tension between the strongly-suppressed strange sea traditionally preferred by dimuon data, and the less suppressed strange sea favored by LHC W/Z data at small values of x . We saw that the NNLO calculation reduced the scale uncertainties significantly at $x \gtrsim 0.2$. Below that, the NNLO scale variations remained on par with the NLO variations, indicating slower perturbative convergence at small x . However, by studying the NLO and NNLO corrections separately, we found that the NNLO corrections are still generally smaller than the NLO corrections, particularly at larger x .

We also considered the impact of new channels that open at NNLO. Most of these are, however, completely negligible for dimuon production. Only the channels initiated by the up or down quark, both of which have a large valence contribution, had a discernable contribution in antineutrino scattering. In the end, however, the bulk of the NNLO contributions arose from corrections to channels already available at NLO. As no NNLO FFs that are applicable to our calculation currently exist, we had to resort to approximative NNLO FFs based on pre-existing NLO fits. A modern NNLO FF fit with proper uncertainty analysis would be beneficial to study the impact and uncertainties associated with the charm-quark fragmentation when using dimuon data in global fits of PDFs. While we expect the NNLO-level mass corrections not included in the presented calculation to be subleading in the $Q^2 \gtrsim 4 \text{ GeV}^2$ region, a full GM-VFNS calculation would still be needed to reduce the remaining dependence on the adopted GM-VFNS variant. In principle, the FFNS NNLO coefficient functions are already known [66], making this a feasible future extension. Other ways to improve the setup presented here is to consider radiative electroweak and target-mass corrections, both of which are known to carry importance in neutrino DIS [80].

The code used for the numerical results presented in this paper will be available from ref. [81] and will also include precomputed interpolation tables enabling an efficient use of our results in global fits of PDFs.

Acknowledgements

We thank F. Hekhorn for the help with the EKO package. We acknowledge the financing from the Magnus Ehrnrooth foundation (S.Y.), the Research Council of Finland Project No. 361179 (I.H.), and the Center of Excellence in Quark Matter of the Research Council of Finland, project 364194. We acknowledge grants of computer capacity from the Finnish IT Center for Science (CSC), under the project jyy2580.

References

- [1] K. Kovařík, P.M. Nadolsky and D.E. Soper, *Hadronic structure in high-energy collisions*, *Rev. Mod. Phys.* **92** (2020) 045003 [[1905.06957](#)].
- [2] J.J. Ethier and E.R. Nocera, *Parton Distributions in Nucleons and Nuclei*, *Ann. Rev. Nucl. Part. Sci.* **70** (2020) 43 [[2001.07722](#)].
- [3] M. Klasen and H. Paukkunen, *Nuclear PDFs After the First Decade of LHC Data*, *Ann. Rev. Nucl. Part. Sci.* **74** (2024) 49 [[2311.00450](#)].
- [4] A. Metz and A. Vossen, *Parton Fragmentation Functions*, *Prog. Part. Nucl. Phys.* **91** (2016) 136 [[1607.02521](#)].
- [5] J.C. Collins, D.E. Soper and G.F. Sterman, *Factorization of Hard Processes in QCD*, *Adv. Ser. Direct. High Energy Phys.* **5** (1989) 1 [[hep-ph/0409313](#)].
- [6] H.-W. Lin et al., *Parton distributions and lattice QCD calculations: a community white paper*, *Prog. Part. Nucl. Phys.* **100** (2018) 107 [[1711.07916](#)].
- [7] M. Constantinou et al., *Parton distributions and lattice-QCD calculations: Toward 3D structure*, *Prog. Part. Nucl. Phys.* **121** (2021) 103908 [[2006.08636](#)].
- [8] S. Alekhin, J. Blümlein, S. Moch and R. Placakyte, *Parton distribution functions, α_s , and heavy-quark masses for LHC Run II*, *Phys. Rev. D* **96** (2017) 014011 [[1701.05838](#)].
- [9] T.-J. Hou et al., *New CTEQ global analysis of quantum chromodynamics with high-precision data from the LHC*, *Phys. Rev. D* **103** (2021) 014013 [[1912.10053](#)].
- [10] S. Bailey, T. Cridge, L.A. Harland-Lang, A.D. Martin and R.S. Thorne, *Parton distributions from LHC, HERA, Tevatron and fixed target data: MSHT20 PDFs*, *Eur. Phys. J. C* **81** (2021) 341 [[2012.04684](#)].
- [11] NNPDF collaboration, *The path to proton structure at 1% accuracy*, *Eur. Phys. J. C* **82** (2022) 428 [[2109.02653](#)].
- [12] ATLAS collaboration, *Determination of the parton distribution functions of the proton using diverse ATLAS data from pp collisions at $\sqrt{s} = 7, 8$ and 13 TeV*, *Eur. Phys. J. C* **82** (2022) 438 [[2112.11266](#)].
- [13] J. McGowan, T. Cridge, L.A. Harland-Lang and R.S. Thorne, *Approximate N^3 LO parton distribution functions with theoretical uncertainties: MSHT20a N^3 LO PDFs*, *Eur. Phys. J. C* **83** (2023) 185 [[2207.04739](#)].
- [14] NNPDF collaboration, *The path to N^3 LO parton distributions*, *Eur. Phys. J. C* **84** (2024) 659 [[2402.18635](#)].
- [15] A. Ablat et al., *CT25: Progress toward next-generation PDFs for precision phenomenology at the LHC*, 12, 2025 [[2512.19779](#)].
- [16] T. Cridge, L.A. Harland-Lang and R.S. Thorne, *Approximate N^3 LO PDFs: Updates and Consequences for Phenomenology*, *PoS DIS2025* (2025) 027 [[2510.09321](#)].
- [17] P. Duwentäster, T. Ježo, M. Klasen, K. Kovařík, A. Kusina, K.F. Muzakka et al., *Impact of heavy quark and quarkonium data on nuclear gluon PDFs*, *Phys. Rev. D* **105** (2022) 114043 [[2204.09982](#)].
- [18] K.J. Eskola, P. Paakkinen, H. Paukkunen and C.A. Salgado, *EPPS21: a global QCD analysis of nuclear PDFs*, *Eur. Phys. J. C* **82** (2022) 413 [[2112.12462](#)].

- [19] R. Abdul Khalek, R. Gauld, T. Giani, E.R. Nocera, T.R. Rabemananjara and J. Rojo, *nNNPDF3.0: evidence for a modified partonic structure in heavy nuclei*, *Eur. Phys. J. C* **82** (2022) 507 [2201.12363].
- [20] NNPDF collaboration, *Nuclear parton distributions from lepton-nucleus scattering and the impact of an electron-ion collider*, *Eur. Phys. J. C* **79** (2019) 471 [1904.00018].
- [21] H. Khanpour, M. Soleymaninia, S. Atashbar Tehrani, H. Spiesberger and V. Guzey, *Nuclear parton distribution functions with uncertainties in a general mass variable flavor number scheme*, *Phys. Rev. D* **104** (2021) 034010 [2010.00555].
- [22] I. Helenius, M. Walt and W. Vogelsang, *NNLO nuclear parton distribution functions with electroweak-boson production data from the LHC*, *Phys. Rev. D* **105** (2022) 094031 [2112.11904].
- [23] J.M. Cruz-Martinez, M. Fieg, T. Giani, P. Krack, T. Mäkelä, T.R. Rabemananjara et al., *The LHC as a Neutrino-Ion Collider*, *Eur. Phys. J. C* **84** (2024) 369 [2309.09581].
- [24] A. Ariga, J. Boyd, F. Kling and A. De Roeck, *Neutrino Experiments at the Large Hadron Collider*, *Ann. Rev. Nucl. Part. Sci.* **75** (2025) 57 [2501.10078].
- [25] FASER collaboration, *Detecting and Studying High-Energy Collider Neutrinos with FASER at the LHC*, *Eur. Phys. J. C* **80** (2020) 61 [1908.02310].
- [26] SND@LHC collaboration, *SND@LHC: the scattering and neutrino detector at the LHC*, *JINST* **19** (2024) P05067 [2210.02784].
- [27] J.L. Feng et al., *The Forward Physics Facility at the High-Luminosity LHC*, *J. Phys. G* **50** (2023) 030501 [2203.05090].
- [28] S. Alekhin et al., *A facility to Search for Hidden Particles at the CERN SPS: the SHiP physics case*, *Rept. Prog. Phys.* **79** (2016) 124201 [1504.04855].
- [29] SHiP, HI-ECN3 PROJECT TEAM collaboration, *SHiP experiment at the SPS Beam Dump Facility*, [2504.06692](#).
- [30] FPF collaboration, *Letter of Intent: The Forward Physics Facility*, [2510.26260](#).
- [31] R. Abdul Khalek et al., *Snowmass 2021 White Paper: Electron Ion Collider for High Energy Physics*, [2203.13199](#).
- [32] CCFR collaboration, *Determination of the strange quark content of the nucleon from a next-to-leading order QCD analysis of neutrino charm production*, *Z. Phys. C* **65** (1995) 189 [hep-ex/9406007].
- [33] NuTeV collaboration, *Precise Measurement of Dimuon Production Cross-Sections in ν_μ Fe and $\bar{\nu}_\mu$ Fe Deep Inelastic Scattering at the Tevatron.*, *Phys. Rev. D* **64** (2001) 112006 [hep-ex/0102049].
- [34] NuTeV collaboration, *Measurement of the Nucleon Strange-Antistrange Asymmetry at Next-to-Leading Order in QCD from NuTeV Dimuon Data*, *Phys. Rev. Lett.* **99** (2007) 192001.
- [35] CHORUS collaboration, *Leading order analysis of neutrino induced dimuon events in the CHORUS experiment*, *Nucl. Phys. B* **798** (2008) 1 [0804.1869].
- [36] NOMAD collaboration, *A Precision Measurement of Charm Dimuon Production in Neutrino Interactions from the NOMAD Experiment*, *Nucl. Phys. B* **876** (2013) 339 [1308.4750].

- [37] A. Kusina, T. Stavreva, S. Berge, F.I. Olness, I. Schienbein, K. Kovarik et al., *Strange Quark PDFs and Implications for Drell-Yan Boson Production at the LHC*, *Phys. Rev. D* **85** (2012) 094028 [[1203.1290](#)].
- [38] G. Bevilacqua, M.V. Garzelli, A. Kardos and L. Toth, *W + charm production with massive c quarks in PowHel*, *JHEP* **04** (2022) 056 [[2106.11261](#)].
- [39] T. Generet, R. Poncelet and M. Muškinja, *Associated production of a W-boson and a charm meson at NNLO in QCD*, *JHEP* **02** (2026) 023 [[2510.24525](#)].
- [40] HERMES collaboration, *Reevaluation of the parton distribution of strange quarks in the nucleon*, *Phys. Rev. D* **89** (2014) 097101 [[1312.7028](#)].
- [41] I. Borsari, R. Sassot and M. Stratmann, *Probing the Sea Quark Content of the Proton with One-Particle-Inclusive Processes*, *Phys. Rev. D* **96** (2017) 094020 [[1708.01630](#)].
- [42] JAM collaboration, *Strange quark suppression from a simultaneous Monte Carlo analysis of parton distributions and fragmentation functions*, *Phys. Rev. D* **101** (2020) 074020 [[1905.03788](#)].
- [43] ATLAS collaboration, *Determination of the strange quark density of the proton from ATLAS measurements of the $W \rightarrow \ell\nu$ and $Z \rightarrow \ell\ell$ cross sections*, *Phys. Rev. Lett.* **109** (2012) 012001 [[1203.4051](#)].
- [44] ATLAS collaboration, *Precision measurement and interpretation of inclusive W^+ , W^- and Z/γ^* production cross sections with the ATLAS detector*, *Eur. Phys. J. C* **77** (2017) 367 [[1612.03016](#)].
- [45] A.M. Cooper-Sarkar and K. Wichmann, *QCD analysis of the ATLAS and CMS W^\pm and Z cross-section measurements and implications for the strange sea density*, *Phys. Rev. D* **98** (2018) 014027 [[1803.00968](#)].
- [46] NNPDF collaboration, *Parton distributions from high-precision collider data*, *Eur. Phys. J. C* **77** (2017) 663 [[1706.00428](#)].
- [47] F. Faura, S. Iranipour, E.R. Nocera, J. Rojo and M. Ubiali, *The Strangest Proton?*, *Eur. Phys. J. C* **80** (2020) 1168 [[2009.00014](#)].
- [48] V.N. Gribov and L.N. Lipatov, *Deep inelastic e p scattering in perturbation theory*, *Sov. J. Nucl. Phys.* **15** (1972) 438.
- [49] V.N. Gribov and L.N. Lipatov, *e^+e^- pair annihilation and deep inelastic e p scattering in perturbation theory*, *Sov. J. Nucl. Phys.* **15** (1972) 675.
- [50] Y.L. Dokshitzer, *Calculation of the Structure Functions for Deep Inelastic Scattering and e^+e^- Annihilation by Perturbation Theory in Quantum Chromodynamics.*, *Sov. Phys. JETP* **46** (1977) 641.
- [51] G. Altarelli and G. Parisi, *Asymptotic Freedom in Parton Language*, *Nucl. Phys. B* **126** (1977) 298.
- [52] D.A. Mason, *Measurement of the strange - antistrange asymmetry at NLO in QCD from NuTeV dimuon data*, Ph.D. thesis, Oregon U., 2006. [10.2172/879078](#).
- [53] F.I. Olness and W.-K. Tung, *When Is a Heavy Quark Not a Parton? Charged Higgs Production and Heavy Quark Mass Effects in the QCD Based Parton Model*, *Nucl. Phys. B* **308** (1988) 813.

- [54] M.A.G. Aivazis, F.I. Olness and W.-K. Tung, *Leptoproduction of heavy quarks. 1. General formalism and kinematics of charged current and neutral current production processes*, *Phys. Rev. D* **50** (1994) 3085 [[hep-ph/9312318](#)].
- [55] M.A.G. Aivazis, J.C. Collins, F.I. Olness and W.-K. Tung, *Leptoproduction of heavy quarks. 2. A Unified QCD formulation of charged and neutral current processes from fixed target to collider energies*, *Phys. Rev. D* **50** (1994) 3102 [[hep-ph/9312319](#)].
- [56] S. Kretzer and I. Schienbein, *Charged current leptoproduction of D mesons in the variable flavor scheme*, *Phys. Rev. D* **56** (1997) 1804 [[hep-ph/9702296](#)].
- [57] J.C. Collins, *Hard scattering factorization with heavy quarks: A General treatment*, *Phys. Rev. D* **58** (1998) 094002 [[hep-ph/9806259](#)].
- [58] M. Krämer, F.I. Olness and D.E. Soper, *Treatment of heavy quarks in deeply inelastic scattering*, *Phys. Rev. D* **62** (2000) 096007 [[hep-ph/0003035](#)].
- [59] W.-K. Tung, S. Kretzer and C. Schmidt, *Open heavy flavor production in QCD: Conceptual framework and implementation issues*, *J. Phys. G* **28** (2002) 983 [[hep-ph/0110247](#)].
- [60] S. Kretzer, H.L. Lai, F.I. Olness and W.K. Tung, *Cteq6 parton distributions with heavy quark mass effects*, *Phys. Rev. D* **69** (2004) 114005 [[hep-ph/0307022](#)].
- [61] R.S. Thorne and W.K. Tung, *PQCD Formulations with Heavy Quark Masses and Global Analysis*, in *HERA and the LHC: 4th Workshop on the Implications of HERA for LHC Physics*, pp. 332–351, 9, 2008 [[0809.0714](#)].
- [62] M. Guzzi, P.M. Nadolsky, H.-L. Lai and C.P. Yuan, *General-Mass Treatment for Deep Inelastic Scattering at Two-Loop Accuracy*, *Phys. Rev. D* **86** (2012) 053005 [[1108.5112](#)].
- [63] J. Gao, T.J. Hobbs, P.M. Nadolsky, C. Sun and C.P. Yuan, *General heavy-flavor mass scheme for charged-current DIS at NNLO and beyond*, *Phys. Rev. D* **105** (2022) L011503 [[2107.00460](#)].
- [64] P. Risse, V. Bertone, T. Ježo, K. Kovařík, A. Kusina, F. Olness et al., *Heavy Quark mass effects in charged-current Deep-Inelastic Scattering at NNLO in the ACOT scheme*, [2504.13317](#).
- [65] E.L. Berger, J. Gao, C.S. Li, Z.L. Liu and H.X. Zhu, *Charm-Quark Production in Deep-Inelastic Neutrino Scattering at Next-to-Next-to-Leading Order in QCD*, *Phys. Rev. Lett.* **116** (2016) 212002 [[1601.05430](#)].
- [66] J. Gao, *Massive charged-current coefficient functions in deep-inelastic scattering at NNLO and impact on strange-quark distributions*, *JHEP* **02** (2018) 026 [[1710.04258](#)].
- [67] S. Forte, E. Laenen, P. Nason and J. Rojo, *Heavy quarks in deep-inelastic scattering*, *Nucl. Phys. B* **834** (2010) 116 [[1001.2312](#)].
- [68] I. Helenius, H. Paukkunen and S. Yrjänheikki, *Dimuons from neutrino-nucleus collisions in the semi-inclusive DIS approach*, *JHEP* **09** (2024) 043 [[2405.12677](#)].
- [69] H. Paukkunen, I. Helenius and S. Yrjänheikki, *Improving the description of dimuon production in neutrino-nucleus collisions using the SACOT- χ scheme*, [2506.09492](#).
- [70] CLEO collaboration, *Absolute Branching Fraction Measurements for D^+ and D^0 Inclusive Semileptonic Decays*, *Phys. Rev. Lett.* **97** (2006) 251801 [[hep-ex/0604044](#)].
- [71] L. Bonino, T. Gehrmann, M. Löchner, K. Schönwald and G. Stagnitto, *Neutral and charged*

current semi-inclusive deep-inelastic scattering at NNLO QCD, *JHEP* **10** (2025) 016 [[2506.19926](#)].

- [72] P.M. Nadolsky and W.-K. Tung, *Improved Formulation of Global QCD Analysis with Zero-mass Matrix Elements*, *Phys. Rev. D* **79** (2009) 113014 [[0903.2667](#)].
- [73] M. Salajegheh, S.M. Moosavi Nejad, M. Soleymaninia, H. Khanpour and S. Atashbar Tehrani, *NNLO charmed-meson fragmentation functions and their uncertainties in the presence of meson mass corrections*, *Eur. Phys. J. C* **79** (2019) 999 [[1904.09832](#)].
- [74] T. Kneesch, B.A. Kniehl, G. Kramer and I. Schienbein, *Charmed-meson fragmentation functions with finite-mass corrections*, *Nucl. Phys. B* **799** (2008) 34 [[0712.0481](#)].
- [75] B.A. Kniehl and G. Kramer, *Charmed-hadron fragmentation functions from CERN LEP1 revisited*, *Phys. Rev. D* **74** (2006) 037502 [[hep-ph/0607306](#)].
- [76] A. Candido, F. Hekhorn and G. Magni, *EKO: evolution kernel operators*, *Eur. Phys. J. C* **82** (2022) 976 [[2202.02338](#)].
- [77] A. Barontini, A. Candido, J. Cruz-Martinez, T. Giani, F. Hekhorn, G. Magni et al., *NNPDF/eko: v0.15.3*, Zenodo (Feb., 2026), [10.5281/zenodo.18493684](#).
- [78] C. Biello and L. Bonino, *Time-Like heavy-flavour thresholds for fragmentation functions: the light-quark matching condition at NNLO*, *Eur. Phys. J. C* **84** (2024) 1192 [[2407.07623](#)].
- [79] A. Candido, S. Forte and F. Hekhorn, *Can $\overline{\text{MS}}$ parton distributions be negative?*, *JHEP* **11** (2020) 129 [[2006.07377](#)].
- [80] H. Paukkunen and C.A. Salgado, *Compatibility of neutrino DIS data and global analyses of parton distribution functions*, *JHEP* **07** (2010) 032 [[1004.3140](#)].
- [81] S. Yrjänheikki, *Code for calculating dimuon production cross sections in neutrino-nucleus collisions*, Zenodo [10.5281/zenodo.18890043](#).